A numerical method for the simulation of free surface flows of viscoplastic fluid in 3D *

Kirill D. Nikitin† Maxim A. Olshanskii‡ Kirill M. Terekhov§ Yuri V. Vassilevski¶

Abstract

In this paper we study a numerical method for the simulation of free surface flows of viscoplastic (Herschel-Bulkley) fluids. The approach is based on the level set method for capturing the free surface evolution and on locally refined and dynamically adapted octree cartesian staggered grids for the discretization of fluid and level set equations. A regularized model is applied to handle the non-differentiability of the constitutive relations. We consider an extension of the stable approximation of the Newtonian flow equations on staggered grid to approximate the visoplastic model and level-set equations if the free boundary evolves and the mesh is dynamically refined or coarsened. The numerical method is first validated for a Newtonian case. In this case, the convergence of numerical solutions is observed towards experimental data when the mesh is refined. Further we compute several 3D viscoplastic Herschel-Bulkley fluid flows over incline planes for the dam-break problem. The qualitative comparison of numerical solutions is done versus experimental investigations. Another numerical example is given by computing the freely oscillating viscoplastic droplet, where the motion of fluid is driven by the surface tension forces. Altogether the considered techniques and algorithms (the level-set method, compact discretizations on dynamically adapted octree cartesian grids, regularization, and the surface tension forces approximation) result in efficient approach to modeling viscoplastic free-surface flows in possibly complex 3D geometries.

1 Introduction

Free surfaces flows of yield stress fluids are common in nature: lava flows, snow avalanches and debris flows, as well as in engineering applications: flows of melt metal, fresh concrete, pastes and other concentrated suspensions [3, 43]. Although the rheology of such materials can be quite complicated, viscoplastic models, for example the Herschel-Bulkley model, are often used to describe the strain rate – stress tensor relationship and predict the fluids dynamics with reasonable accuracy, see e.g. [14, 19, 30, 54]. Modeling such phenomena numerically is a challenging task due to the non-trivial coupling of complex flow dynamics and free surface evolution. Substantial progress has been made during the last two decades in developing efficient and accurate numerical methods for computing flows with free surfaces and interfaces, see e.g. [53, 55, 60] and references therein. The level set method is an implicit surface-capturing technique [57] which was proved to be particular efficient for handling free surfaces which may undergo complex topological changes. The method is extensively used for numerical modeling of free-surface flows with finite difference [44, 46], finite volume [27] and finite element [8, 9] methods as discretization techniques. Most of this research has been focused on application to Newtonian free-surface and interface flows.

Numerical simulations of viscoplastic fluid flow has already attracted a lot of attention, see for example the review papers [18, 22]. Yet the accurate modeling of free-surface viscoplastic fluid flows poses a serious challenge. The previous studies include the application of the Arbitrary Langrangian–Eulerian method for free-surface tracking of axisymmetric squeezing Bingham flows [33], volume of fluid surface tracking for 2D Bingham

*This work has been supported in part by RFBR grants 09-01-00115, 11-01-00971 and the federal program "Scientific and scientific-pedagogical personnel of innovative Russia".

†Institute of Numerical Mathematics, Russian Academy of Sciences, Moscow; nikitin.kira@gmail.com

‡Department of Mechanics and Mathematics, Moscow State University, Moscow; Maxim.Olshanskii@mtu-net.ru; www.mathcs.emory.edu/~molshan

§Institute of Numerical Mathematics, Russian Academy of Sciences, Moscow; kirill.terehov@gmail.com

¶Institute of Numerical Mathematics, Russian Academy of Sciences, Moscow; yuri.vassilevski@gmail.com

flows [2], the free interface lattice Boltzmann model [26], the simulation of viscoplastic fluids over incline planes in shallow layer approximations [4, 6, 32]. The present paper develops a numerical method for simulation of complex 3D viscoplastic fluid flows based on the free surface capturing by the level set method.

The numerical methodology studied here is based on several other important ingredients, besides the level set method. To approximate complex geometries emerging in the process of the free surface evolutions we use adaptive cartesian grids dynamically refined near the free surfaces and coarsened in the fluid interior. We note that using grids adaptively refined towards the free surface is a common practice, e.g. [11, 27]. Although much of the adaptive methods studied in the literature are based on locally refined triangulations (tetrahedra) and finite element discretizations, e.g. [11, 21], adaptive (octree) cartesian grids are often more convenient for frequent and routine executions of refining / coarsening procedures in the course of time integration. For the application of such grids in image processing, the visualization of amorphous medium, free surface Newtonian flow computations and other applications where non-trivial geometries occur see [38, 40, 41, 44, 49, 56, 59]. We combine the mesh adaptation with a splitting algorithm for time integration. The splitting scheme decouples each time step into separate advection, plasticity, div-free correction, and level-set function update substeps. For the sake of adaptation, the grid is dynamically refined or coarsened according to the distance to the evolving free boundary on every time step. For the space discretization we use a finite difference method on octree cartesian meshes with the staggered allocation of velocity–pressure nodes. Further important ingredients of the algorithm, the preserving of the distance property of the discrete level set functions, and the approximation of the normal vectors and the curvatures of the free surface, are briefly discussed. For details we refer to [45].

The remainder of the paper is organized as follows. Section 2 reviews the mathematical model. In section 3 we discuss the details of the numerical approach: the splitting algorithm for time integration of the coupled system of the Herschel-Bulkley fluid model and the level set function equations, a finite difference method for space discretization, volume correction and re-initialization methods for the level set function. Numerical results for several 3D test problems are presented in section 4. Numerical tests include the Newtonian broken dam problem, the viscoplastic Herschel-Bulkley fluid flow over incline planes and freely oscillating viscoplastic droplet. Section 5 contains some closing remarks.

2 Mathematical model

We consider the Herschel-Bulkley model of a viscoplastic non-Newtonian incompressible fluid flow in a bounded time-dependent domain $\Omega(t) \in \mathbb{R}^3$. We assume that $\overline{\partial\Omega(t)} = \overline{\Gamma_D} \cup \overline{\Gamma(t)}$, where Γ_D is the static boundary[1] (walls) and $\Gamma(t)$ is a free surface. In the time interval $(0, T]$, the fluid flow is described by the fluid equations

$$\begin{cases} \rho\left(\dfrac{\partial \mathbf{u}}{\partial t} + (\mathbf{u}\cdot\nabla)\mathbf{u}\right) - \mathbf{div}\ \boldsymbol{\tau} + \nabla p = \mathbf{f} \\ \nabla\cdot\mathbf{u} = 0 \end{cases} \quad \text{in } \Omega(t), \tag{1}$$

and the Herschel-Bulkley constitutive law

$$\begin{aligned} \boldsymbol{\tau} = \left(K\,|\mathbf{Du}|^{n-1} + \tau_s|\mathbf{Du}|^{-1}\right)\mathbf{Du} \ &\Leftrightarrow\ |\boldsymbol{\tau}| > \tau_s, \\ \mathbf{Du} = \mathbf{0} \ &\Leftrightarrow\ |\boldsymbol{\tau}| \le \tau_s, \end{aligned} \tag{2}$$

where $\mathbf{u}, p, \boldsymbol{\tau}$ are velocity vector, pressure and the deviatoric part of the stress tensor, K is the consistency parameter, τ_s is the yield stress parameter, n is the flow index, for $n < 1$ the fluid is shear-thinning, for $n > 1$ is shear-thickening, and $n = 1$ corresponds to the classic case of the Bingham plastic, ρ is the density of fluid, $\mathbf{Du} = \frac{1}{2}[\nabla\mathbf{u} + (\nabla\mathbf{u})^T]$ is the rate of strain tensor and $|\mathbf{Du}| = \big(\sum_{1\le i,j\le 3} |D_{ij}\mathbf{u}|^2\big)^{\frac{1}{2}}$, $\mathbf{div}$ denotes the vector divergence operator. Thus the medium behaves like a fluid in the domain where $|\mathbf{Du}| \neq 0$, the so-called *flow region*, and exhibits the rigid body behavior in the region where the stresses do not exceed the threshold parameter τ_s, the so-called *rigid (or plug) region*. One of the difficult features of the problem is that two regions are unknown *a priori*. Since the stress tensor is indeterminate in the plug region, in [20] it was

[1] The Γ_D part of the boundary may vary in time, although remaining static, see e.g. the dam break problem from Sec. 4.1.

pointed out that (formally) the equations (1) make sense only on those parts of the domain where $|\mathbf{Du}| \neq 0$ and the mathematically sound formulation of (1)–(2) can be written in terms of variational inequalities. Another common way to avoid this difficulty in practice, is to regularize the problem by enforcing the fluidic medium behavior in the entire computational domain (see e.g. [10, 22, 48]). Adopting this approach we replace $|\mathbf{Du}|$ with $|\mathbf{Du}|_\varepsilon = \sqrt{|\mathbf{Du}|^2 + \varepsilon^2}$ for a *small* parameter $\varepsilon > 0$. This allows us to pose equations in the entire domain:

$$\begin{cases} \rho\left(\dfrac{\partial \mathbf{u}}{\partial t} + (\mathbf{u}\cdot\nabla)\mathbf{u}\right) - \mathbf{div}\ \mu_\varepsilon \mathbf{Du} + \nabla p = \mathbf{f} \\ \nabla \cdot \mathbf{u} = 0 \end{cases} \quad \text{in } \Omega(t), \tag{3}$$

with the shear-dependent effective viscosity

$$\mu_\varepsilon = K\,|\mathbf{Du}|_\varepsilon^{n-1} + \tau_s |\mathbf{Du}|_\varepsilon^{-1}.$$

At the initial time $t = 0$ the domain and the velocity field are known:

$$\Omega(0) = \Omega_0, \quad \mathbf{u}|_{t=0} = \mathbf{u}_0. \tag{4}$$

On the static part of the flow boundary we assume the velocity field satisfies Dirichlet boundary condition

$$\mathbf{u} = \mathbf{g} \quad \text{on } \Gamma_D, \tag{5}$$

$\mathbf{g}$ is given. On the free surface $\Gamma(t)$, we impose the kinematic condition

$$v_\Gamma = \mathbf{u}|_\Gamma \cdot \mathbf{n}_\Gamma \tag{6}$$

where $\mathbf{n}_\Gamma$ is the normal vector for $\Gamma(t)$ and v_Γ is the normal velocity of the free surface $\Gamma(t)$. Balancing the surface tension and stress forces yields the second condition on $\Gamma(t)$:

$$\boldsymbol{\sigma}_\varepsilon \mathbf{n}_\Gamma = \varsigma \kappa \mathbf{n}_\Gamma - p_{\text{ext}} \mathbf{n}_\Gamma \quad \text{on } \Gamma(t), \tag{7}$$

where $\boldsymbol{\sigma}_\varepsilon = \mu_\varepsilon \mathbf{Du} - p\,\mathbf{I}$ is the regularized stress tensor of the fluid, κ is the sum of the principal curvatures, ς is the surface tension coefficient, p_{ext} is an exterior pressure which we assume to be zero, $p_{\text{ext}} = 0$.

Existing numerical approaches to the numerical solution of (3)-(7) can be roughly divided into two groups: methods based on surface tracking and those which use surface capturing. Free surface tracking algorithms are based on the surface evolution equation (6). We employ the surface capturing algorithm based on the implicit definition of $\Gamma(t)$ as the zero level of a globally defined function $\phi(t, \mathbf{x})$. A smooth (at least Lipschitz continuous) function ϕ such that

$$\phi(t,\mathbf{x}) = \begin{cases} < 0 & \text{if } \mathbf{x} \in \Omega(t) \\ > 0 & \text{if } \mathbf{x} \in \mathbb{R}^3 \setminus \overline{\Omega(t)} \\ = 0 & \text{if } \mathbf{x} \in \Gamma(t) \end{cases} \qquad \text{for all } t \in [0,T]$$

is called the *level set* function. The initial condition (4) allows us to define $\phi(0, \mathbf{x})$. For $t > 0$ the level set function satisfies the following transport equation [46]:

$$\frac{\partial \phi}{\partial t} + \widetilde{\mathbf{u}} \cdot \nabla \phi = 0 \quad \text{in } \mathbb{R}^3 \times (0, T] \tag{8}$$

where $\widetilde{\mathbf{u}}$ is any smooth velocity field such that $\widetilde{\mathbf{u}} = \mathbf{u}$ on $\Gamma(t)$. The employed mathematical model consists of equations (3), (4), (5), (7), and (8). We note that the implicit definition of $\Gamma(t)$ as zero level of a globally defined function ϕ leads to numerical algorithms which can easily handle complex topological changes of the free surface such as merging or pinching of two fronts and formation of singularities. The level set function provides an easy access to useful geometric characteristics of $\Gamma(t)$. For instance, the unit outward normal to $\Gamma(t)$ is $\mathbf{n}_\Gamma = \nabla\phi/|\nabla\phi|$, and the surface curvature is $\kappa = \nabla \cdot \mathbf{n}_\Gamma$. From the numerical point of view, it is often beneficial if the level set function possesses the signed distance property, i.e. it satisfies the Eikonal equation

$$|\nabla \phi| = 1. \tag{9}$$

3 Numerical method

The numerical method is built on the approach developed in [44, 45] for the Newtonian flows. Below we describe important steps of the numerical procedure and discretization, while missing details can be found in [45].

3.1 Time integration

Various numerical methods have been proposed for the time integration of the fluid equations, ranging from fully implicit schemes to fractional steps methods. Here we apply a semi-implicit splitting method that avoids nested iteration loops and extends the well-known approach of Chorin-Temam-Yanenko, see e.g. [12, 46].

Each time step of the method (given $\mathbf{u}(t)$, $p(t)$, $\phi(t)$ find approximations to $\mathbf{u}(t+\Delta t)$, $p(t+\Delta t)$, $\phi(t+\Delta t)$) consists of the following substeps. For the sake of presentation simplicity, we suppress spacial discretization details in this section. The spacial discretization of all involved operators will be discussed in the next section.

Level set part: $\Omega(t) \to \Omega(t+\Delta t)$

1. Extend velocity to the exterior of fluid body: $\mathbf{u}(t)|_{\Omega(t)} \to \widetilde{\mathbf{u}}(t)|_{\mathbb{R}^3}$, see section 3.2. In practice, the extension is performed to a bulk computational domain, rather than $\mathbb{R}^3$.

2. Find $\phi(t+\Delta t)$ from (8) by a numerical integration with the semi-Lagrangian method [58] and using the extended velocity field. This is done in few substeps: First, for every grid point $\mathbf{y}$, solve the characteristic equation backward in time

$$\frac{\partial \mathbf{x}(\tau)}{\partial \tau} = \widetilde{\mathbf{u}}(\mathbf{x}(\tau), \tau), \quad \mathbf{x}(t+\Delta t) = \mathbf{y}, \quad \text{for } \tau \in [t+\Delta t, t]. \tag{10}$$

   The characteristic equation is integrated numerically with the second order accuracy. Second, assign

$$\phi^*(\mathbf{y}, t+\Delta t) = \phi(\mathbf{x}(t), t). \tag{11}$$

   To compute $\phi(\mathbf{x}(t), t)$ and velocity values along numerical characteristics an interpolation is used. At this step the signed distance property of ϕ and the volume balance may be lost.

3. Perform the correction $\phi^*(t+\Delta t) \to \widehat{\phi}^*(t+\Delta t)$ in order to enforce the global volume conservation, see section 3.3;

4. Re-initialize the level set function $\widehat{\phi}^*(t+\Delta t) \to \phi(t+\Delta t)$ so that $\phi(t+\Delta t)$ (approximately) satisfies (9). The re-initialization procedure is discussed in section 3.3.

When the "level set" part of the splitting algorithm is complete, the computed $\phi(t+\Delta t)$ implicitly defines the new fluid domain $\Omega(t+\Delta t)$.

Remeshing. Given the new fluid domain we update and adapt the grid accounting for the new position of the free surface. The details of the remeshing procedure are given in section 3.2.

Re-interpolation. Now we re-interpolate all discrete variables to the new grid. Note that the re-interpolated velocity field is defined globally (due to the extension procedure at the beginning of the level-set part).

Fluid part: $\{\mathbf{u}(t), p(t)\} \to \{\mathbf{u}(t+\Delta t), p(t+\Delta t)\}$. We find the new velocity and pressure in several steps. First we perform a pure advection step by the semi-Lagrangian method, next we add viscous terms, and finally we project the velocity into (discretely) divergence-free functions subspace and recover new pressure:

1. For each velocity component u_k, $k = 1, 2, 3$, we apply the semi-Lagrangian method similar to the case of the level set function as described above. The only differences are the following: now $\mathbf{y}$ denotes not a cell vertex, but a node where particular velocity component is defined, and (11) is replaced by

$$u_k^*(\mathbf{y}, t+\Delta t) = \widetilde{u}_k(\mathbf{x}(t), t). \tag{12}$$

2. The viscoplastic step:

$$\widehat{\mathbf{u}}^*(t+\Delta t) = \mathbf{u}^*(t+\Delta t) + \rho^{-1}\Delta t \left[\mathbf{div}\, \left(K\,|\mathbf{D}\widetilde{\mathbf{u}}(t)|_{\varepsilon}^{n-1} + \tau_s|\mathbf{D}\widetilde{\mathbf{u}}(t)|_{\varepsilon}^{-1}\right)\mathbf{D}\widetilde{\mathbf{u}}(t) + \mathbf{f}(t)\right] \tag{13}$$

When this step is realized numerically, the discretization of the viscous terms in the next to the boundary nodes needs some boundary conditions for $\widetilde{\mathbf{u}}(t)$. On the 'static' boundary we use conditions (5). We split the surface tension balance condition (7) between the projection step (14) and the viscous step (13), so the velocity update in (13) uses the strain-free condition: $[\mathbf{D}\widetilde{\mathbf{u}}(t)]\mathbf{n}_\Gamma|_{\Gamma(t)} = 0$ on the free boundary.

3. The projection step: Solve for pressure $p(t+\Delta t)$:

$$\begin{cases} \nabla\cdot\nabla p(t+\Delta t) = \dfrac{1}{\Delta t}\nabla\cdot\widehat{\mathbf{u}}^*(t+\Delta t) \quad \text{in } \Omega(t+\Delta t), \\ p(t+\Delta t) = \rho^{-1}\varsigma\kappa(t+\Delta t) \quad \text{on } \Gamma(t+\Delta t) \quad \text{and} \quad \dfrac{\partial p(t+\Delta t)}{\partial \mathbf{n}} = 0 \quad \text{on } \Gamma_D. \end{cases} \tag{14}$$

Update velocity

$$\mathbf{u}(t+\Delta t) = \widehat{\mathbf{u}}^*(t+\Delta t) - \Delta t\nabla p(t+\Delta t).$$

Goto the level set part.

3.2 Mesh adaptation and discretization

A possibly complex geometry of the free surface and the accurate approximation of the surface tension forces require a sufficiently fine grid in a neighborhood of $\Gamma(t)$. In this case, the use of uniform grids becomes prohibitively expensive, especially in 3D. Locally refined meshes often need considerably less computational resources. However, such meshes have to be dynamically refined and coarsened if the free surface evolves. The remeshing is, in general, CPU time and memory demanding procedure for consistent regular tetrahedrizations. This step becomes considerably less expensive if one uses cartesian octree meshes with cubic cells. The two-dimensional analog of an octree mesh refined towards free surface is illustrated in Figure 1. More details on quadtree/octree data structures can be found in [51, 52]. The use of cubic cells is also appealing due to the straightforward data interpolation between two consecutive meshes.

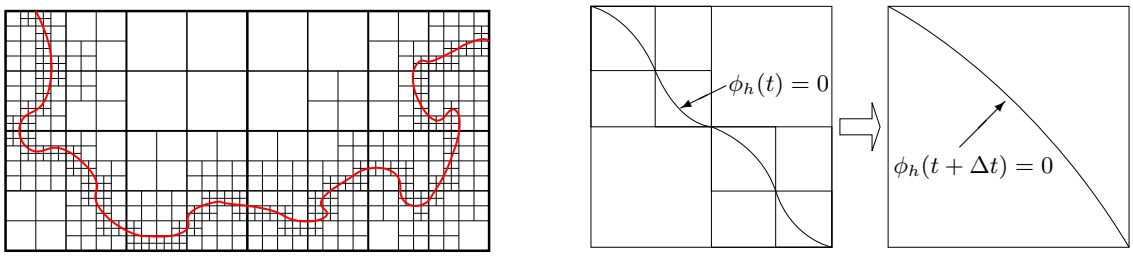

Figure 1: Left: 2D quadtree grid adapted to free boundary. Right: The loss of discrete free surface geometric information when ϕ_h is transported from a region with a finer mesh to the one with a coarser mesh

Our adaptation strategy is based on the graded refinement (the sizes of two neighboring cells may differ at most by the factor of two) of the mesh towards the *current and predicted* location of the free surface. By the predicted location at time t we mean the one occupied by $\Gamma(t+\Delta t)$ if the characteristic equation (10) is solved with current velocity and Δt. The grid refinement towards the predicted interface location is done in order to reduce the loss of the local surface geometric information which occurs if $\Gamma(t+\Delta t)$ is approximated by a trilinear function on a coarser grid; such possible loss is illustrated in Figure 1. Note, that the predicted location may slightly differ from the actually computed $\Gamma(t+\Delta t)$ in the level set part of the algorithm, since the mesh adaptation step is performed *before* the velocity and Δt are updated in the fluid part of the algorithm. However, this allows us to preserve most of the local surface geometry and avoids double remeshing. In numerical

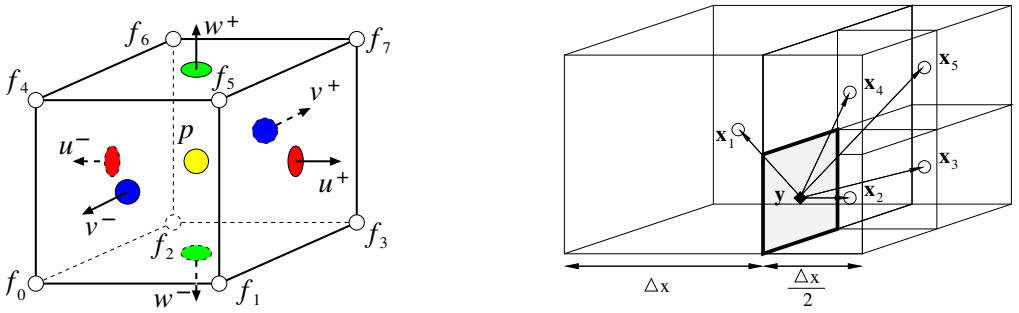

Figure 2: Left: Location of variables in staggered grid; p is pressure, $\{u^{\pm}, v^{\pm}, w^{\pm}\}$ are velocity components, f is nodal scalar function, e.g. the level set function. Right: Discretization stencil for $\partial p/\partial x$.

experiments from the next section all cells intersected by $\Gamma(t)$ or $\Gamma(t + \Delta t)$ have the same width $h_{\min}$. Away from the surface the mesh is aggressively coarsened up to the maximum cell width $h_{\max}$ in the fluid domain $\Omega(t)$ and h_{ext} in the rest of computational domain.

To produce a stable approximation we use the staggered location of velocity and pressure unknowns to discretize the fluid equations [31, 36] (see Figure 2): The pressure is approximated in cell centers, velocity components are approximated in face centers. The level set function is approximated in cell vertices. We discretize differential operators with a FD method using compact node stencils.

The approximation of the velocity divergence in the center $\mathbf{x}_V$ of a fluid grid cell V resembles the finite volume method: Let $\mathcal{F}(V)$ be the set of faces for V, i.e. $\partial V = \cup_{F\in\mathcal{F}(V)} F$, and $\mathbf{y}_F$ denotes the center of $F \in \mathcal{F}(V)$, we define

$$(\mathbf{div}_h\, \mathbf{u}_h)(\mathbf{x}_V) = |V|^{-1} \sum_{F\in\mathcal{F}(V)} |F|(\mathbf{u}_h \cdot \mathbf{n})(\mathbf{y}_F). \tag{15}$$

Thanks to the staggered location of velocity nodes $(\mathbf{u}_h \cdot \mathbf{n})(\mathbf{y}_F)$ is well-defined. One common choice for the discrete pressure gradient is to consider the formal transpose of the discrete divergence operator. On the non-uniform meshes, as in Figure 2 (right), this would lead to a zero order approximation of the gradient. It is sometimes argued that for enclosed flows accurate approximations to velocities are still obtained in this case, since the pressure merely acts as the Lagrange multiplier corresponding to the divergence-free constraint. We found that this choice of the discrete pressure gradient does not work well in our case. The likely explanation is that for free surface flows the pressure is involved in the surface tension forces balance in (7) (see also (14)) and therefore reasonably accurate approximation of pressure is necessary to account for the capillary forces. Thus for every internal cell face we define a corresponding component of the pressure gradient as described below. Since we use graded octree meshes, for any interior cell face there can be only two geometric cases. If the face is shared by two equal cells, the standard central finite difference is used to approximate the corresponding gradient component. If the sizes of the cells sharing the face are different, as shown in Figure 2 (right), the gradient approximation is reduced to the first order: With the notation of Figure 2, the x-component of the gradient operator at the face center $\mathbf{y}$ is approximated by

$$p_x(\mathbf{y}) \approx \frac{1}{3\Delta x}(p_2 + p_3 + p_4 + p_5 - 4p_1). \tag{16}$$

A proper finite difference approximation of the visco-plastic terms is the important part of the scheme. We use the following identity, which is valid for a smooth $\mathbf{u}$ such that $\nabla \cdot \mathbf{u} = 0$:

$$\mathbf{div}\ \mu_\varepsilon \mathbf{D}\mathbf{u} = \frac{1}{2}\left(\mathbf{div}\ \mu_\varepsilon \nabla\mathbf{u} + (\nabla\mathbf{u})^T \nabla\mu_\varepsilon\right)$$

Due to the non-uniform nodes distribution we use a hybrid of meshless finite point [47] and finite difference approach. For a given velocity node $\mathbf{y}$ we consider a set of velocity nodes in an $\mathcal{O}(h)$-neighborhood of $\mathbf{y}$. This set of nodes is defined as follows: it includes $\mathbf{y}$, velocity nodes (for the same component) from two cells sharing $\mathbf{y}$

and all velocity nodes (for the same component) from the cells having a common face, edge or a vertex with these two cells sharing $\mathbf{y}$. By the least square method we find a second order polynomial $P_2(\mathbf{x})$ which interpolates the values of velocity in the given set of nodes. Differentiating P_2 in $\mathbf{x} = \mathbf{y}$ we compute the approximation for $(\nabla \mathbf{u})^T$ in $\mathbf{y}$. Since P_2 is defined in the $\mathcal{O}(h)$-neighborhood of $\mathbf{y}$, the approximation to $\nabla \mathbf{u}$ is also defined in the neighborhood. Hence one can also compute the approximation to μ_ε and $\mu_\varepsilon \nabla \mathbf{u}$ in any point from this neighborhood. Now the approximations to $\mathbf{div}\ \mu_\varepsilon \nabla \mathbf{u}$ and $\nabla \mu_\varepsilon$ in $\mathbf{y}$ are computed by the central differences with step size equal h.

Further, the semi-Lagrangian method needs the interpolation of nodal velocities by a globally defined velocity function. This is done by assigning to an arbitrary point of the flow domain a linear combination of six nodal values as described in detail in [45]. Finally, the extension of $\mathbf{u}_h$ from $\Gamma_h(t)$ to the grid nodes in exterior of fluid domain is performed along the normals. To this end, for a given node $\mathbf{x}$ we find the "nearest" point $\mathbf{y}_\mathbf{x} \in \Gamma_h(t)$ by the following iterative algorithm. Set $\mathbf{y}^0 = \mathbf{x}$, define $\mathbf{y}^{n+1} = \mathbf{y}^n - \alpha \nabla \phi_h(\mathbf{y}^n)$, $n = 0, 1, \ldots$, with a relaxation parameter $\alpha > 0$. The iteration is terminated once $|\mathbf{y}^{n+1} - \mathbf{y}^n| \le \varepsilon$ and we set $\mathbf{y}_\mathbf{x} = \mathbf{y}^{n+1}$, $u_h(\mathbf{x}) = u_h(\mathbf{y}_\mathbf{x})$, where $u_h(\mathbf{y}_\mathbf{x})$ is computed via the interpolation. In our calculations we chose $\varepsilon = 10^{-8}$ and $\alpha = \frac{\sqrt{5}-1}{2}$.

To account for the surface tension forces we need approximations to the free surface normal vectors and curvatures. The unit outward normal can be computed from the level set function: $\mathbf{n}_\Gamma = \nabla\phi/|\nabla\phi|$ on $\Gamma(t)$. We derive the second order approximation of the gradient through the Taylor expansion in all possible combinations of octree cells sharing the node.

The mean curvature of the interface can be defined as the divergence of the normal vector, $\kappa(\phi) = \nabla \cdot \mathbf{n} = \nabla \cdot (\nabla\phi/|\nabla\phi|)$. First, $\nabla_h \phi_h$ is computed in cell vertices and is averaged in face centers. Once $\nabla_h \phi_h / |\nabla_h \phi_h|$ is known in face centers, $\kappa_h(\phi_h) = \nabla_h \cdot \nabla_h \phi_h / |\nabla_h \phi_h|$ is computed in cell centers by standard second order center differences. Since $\nabla\phi$ is computed with second order accuracy, $\kappa(\phi)$ is approximated at least with the first order.

3.3 Volume correction and redistancing

The numerical advection of the free boundary may cause a divergence (loss or gain) of the fluid volume. This divergence is reduced by the grid refinement near free surface and using more accurate time integration of (8), but not eliminated completely. Thus we perform the adjustment of the level set function by adding a suitable constant to preserve the fluid volume. This is done by solving for a constant δ the following equation

$$\mathrm{meas}\{\mathbf{x} : \phi(\mathbf{x}) < \delta\} = Vol^{\mathrm{reference}}$$

and correcting $\phi^{new} = \phi - \delta$. The bisection algorithm was used to find δ and a Monte-Carlo method was applied to evaluate $\mathrm{meas}\{\mathbf{x} : \phi(\mathbf{x}) < \delta\}$.

Both the advection and the volume correction of the level set function may cause the loss of its signed distance property. For the continuous level set function this property can be written in the form of the Eikonal equation:

$$|\nabla \phi(\mathbf{x})| = 1, \quad \mathbf{x} \in \mathbb{R}^3, \tag{17}$$

with the boundary condition on the free surface $\Gamma(t)$:

$$\phi(\mathbf{x}) = 0, \quad \mathbf{x} \in \Gamma(t).$$

The property (17) is important for the computation of the geometric quantities of the free boundary and numerical stability. To recover the signed distance property we perform a redistancing procedure, also known as re-initialization.

The re-initialization is peformed in several steps. First, the location of the discrete interface $\Gamma(t)$ is explicitly recovered from the nodal values of ϕ using the marching cubes technique [35, 37]. The resulting internal surface triangulation turns out to be a conformal triangulation in space. Further, the redistancing procedure is split into two substeps: the assignment of new distance values in the vertices of interface cells (i.e. cells that are intersected with the interface), and finding solution to a discrete counterpart of (17) in all remaining nodes. The second substep is performed by the fast marching method from [1] adapted to octree grids.

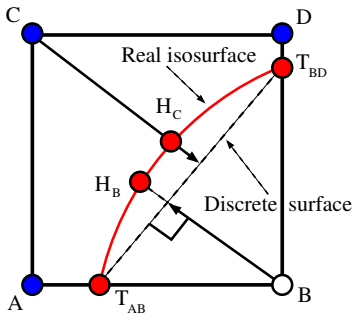

Figure 3: Approximating the distance to the $\{\phi_h(\mathbf{x}) = 0\}$ level set.

To accomplish the first substep we make use of the constructed triangular approximation to the $\{\phi_h(\mathbf{x}) = 0\}$ level set. Note that interface triangulation is only an approximation to the zero level of the piecewise trilinear function ϕ_h. To account for this we proceed as follows. For each surface triangle T and a neighboring grid node $\mathbf{x}$ consider the line passing through $\mathbf{x}$ and orthogonal to the plane of T (see Figure 3 for the 2D illustration). The trace of ϕ_h on the line segment contained in the cell is a cubic function $\psi(t) = f_3t^3 + f_2t^2 + f_1t + f_0$ where $\psi(0) = \phi_h(\mathbf{x})$. The smallest positive root of the equation $\psi(t) = 0$ defines the point $H_{\mathbf{x}}$ where the line crosses the zero isosurface of ϕ_h. If the initial value of $\phi_h(\mathbf{x})$ is greater than the computed distance to $H_{\mathbf{x}}$, we set it equal to this distance. Otherwise we update $\phi_h(\mathbf{x})$ by the distance to $H_{\mathbf{x}}$ if it does not exceed distances to the vertices of the considered triangle.

In [45] it was demonstrated that this re-initialization method produces sufficiently accurate and convergent approximations to the distance function and compares favorably to other re-initialization methods, e.g. to the one from [42]. Application of an accurate re-initialization is important for modeling phenomena driven by the surface tension forces, see the example in section 4.3.

4 Numerical experiments

In this section we present results of several numerical tests. First we validate the code by comparing computed statistics for the Newtonian case with those available in the literature. Further, few results are shown for viscoplastic fluid flows over incline planes and for a freely oscillating viscoplastic droplet.

4.1 The Newtonian broken dam problem

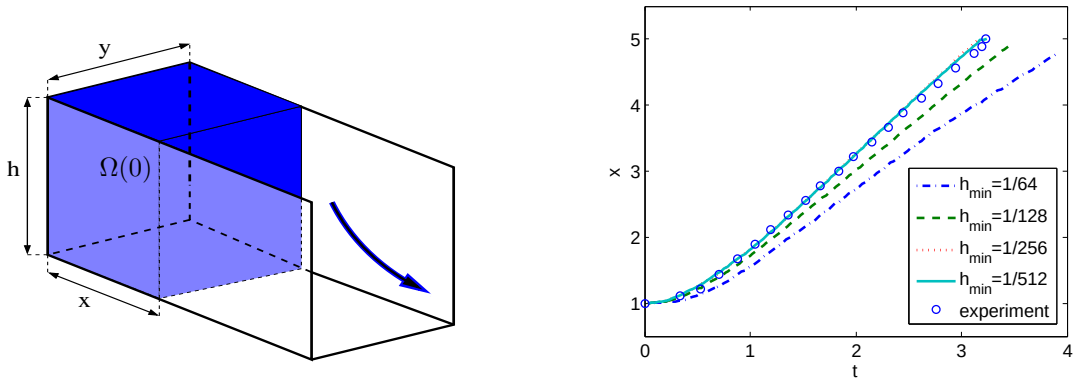

Figure 4: Left: The setup of the 'dam break problem' in numerical simulations; Right: The computed position of the free surface bottom front for the dam break problem versus (shifted) experimental values from [39]. The convergence for decreasing $h_{\min}$ is clearly seen.

This is a classic test case for free surface flows. It was adopted by several researchers as a benchmark test to validate the numerical performance of solves for Newtonian flows with two-liquid interfaces or free-surfaces both in 2D and 3D, see e.g. [15, 16, 24, 61]. The computational problem setup is shown in figure 4 (left). In the initial state, the fluid is placed on the left-hand side as a water column with dimensions $x = y = h = 1$. Further, the water column collapses driven by the gravity force $\mathbf{f} = (0, 0, 1)^T$. On the walls we impose slip boundary conditions: $\mathbf{u} \cdot \mathbf{n} = 0$ and $\mathbf{t}_k \cdot \boldsymbol{\sigma}\mathbf{n} = 0$, where $\boldsymbol{\sigma}$ denotes the stress tensor, $\mathbf{t}_k$, $k = 1, 2$ are tangent vectors. We are interested in the evolution of the free surface front along the bottom wall. This statistic can

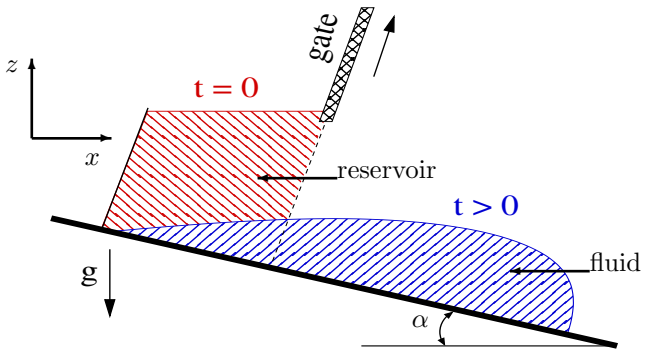

Figure 5: The sketch of the flow configuration.

be compared to the experimental values from [39]. In numerical simulations the values of K, ρ, ς were set to model the viscosity, density, and surface tension of water. For the Newtonian fluid it holds $\tau_s = 0$ and $n = 1$. The numerical results obtained for the horizontal location of the free surface front along the bottom wall are compared to the experimental values from [39] in figure 4 (time and front position are shown dimensionless). The coarsest grid was defined with $h_{\min} = 1/64$, $h_{\max} = 1/32$, $h_{\text{ext}} = 1/16$, fine grids where obtained by refining this mesh gradely. Following [15] we make the -0.007 real seconds (≈ -0.0917 dimensionless seconds) shift of the experimental data to account for the finite time of the dam removal in the life experiment. From the right figure 4 we clearly see the convergence of the computed solutions to the experimental measurements when the grid is refined. The plots of the front position of the computed solutions for $h_{\min} = 1/256$ and $h_{\min} = 1/512$ are visually hard to distinct.

4.2 The Herschel-Bulkley fluid flows over incline planes

Flows of viscoplastic fluids over incline surfaces have a long history in research due to their important role in nature and engineering, see [3, 32] for the review and the comprehensive coverage of the literature on the subject. Mathematical analysis of the problem, including analytical representation of the form of the final arrested state, is available in the special case of two-dimensional shallow layer approximation and low Reynolds numbers [4, 5, 6, 32]. Therefore, in a more general setting, numerical modeling is an important and indispensable research tool for analyzing such types of flows. Earlier numerical studies include computing the dam-break and sloping yield stress fluid flows in the shallow layer approximations (lubrication models), e.g. [4, 6, 7, 32]. In such an approach the effect of inertia and surface tension are often neglected. The method developed in this paper allows to account for true three-dimensionality of the flow as well as for inertia, surface tension, and more complex geometries, no shallow layer assumptions are needed.

In this experiment we consider a plane inclined at angle α to the horizontal. A rectangular reservoir of length X and width Y filled with a volume V of Herschel-Bulkley fluid is placed on the plane. The reservoir is equipped with a gate perpendicular to the slope. When the gate is open, the fluid is released and starts motion driven by the gravity force. The 2D schematic flow configuration is shown in figure 5.

We run numerical experiments with the following set of dimensional parameters which correspond to the experimental setting in [13]: $X = 0.51m$, $Y = 0.3m$, $V = 0.06m^3$, $\alpha \in \{12^o, 18^o\}$, and two sets of Herschel-Bulkley model parameters, $K = 47.68Pas^{-n}$, $n = 0.415$, $\tau_s = 89Pa$ and $K = 75.84Pas^{-n}$, $n = 0.579$, $\tau_s = 109Pa$. The Herschel-Bulkley model with such parameters was found in [13] to approximate the rheology of Carbopol Ultrez 10 gel of 0.30% and 0.40% concentration, respectively. The typical fluid evolution is illustrated in figure 6, where the colors indicate the depth of the flow.

Regarding the flow structure, the existing shallow-layer theory distinguishes the yielding region close to the bottom boundary and the pseudo-plug region, the region where the fluid is weakly yielded and considered solid up to higher order terms with respect to the layer thickness. Pseudo-plugs are predicted to dominate the dynamics over substantial regions of shallow flows. Qualitatively the same structure was observed for the computed 3D solutions and illustrated in figure 7.

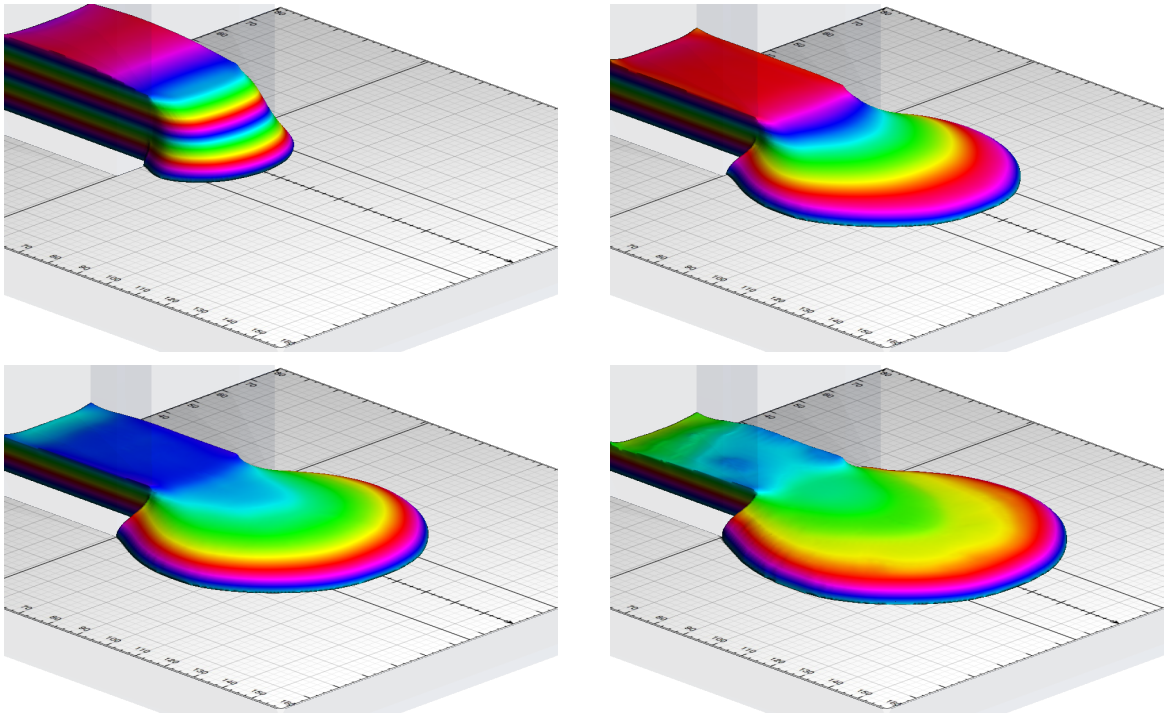

Figure 6: Three-dimensional view of the dam-break flow over incline plane with $\alpha = 12^o$ at times $t \in \{0.2, 0.6, 1.0, 2.0\}s$ with instantaneous gate removal and $K = 47.68Pas^{-n}$, $n = 0.415$, $\tau_s = 89Pa$.

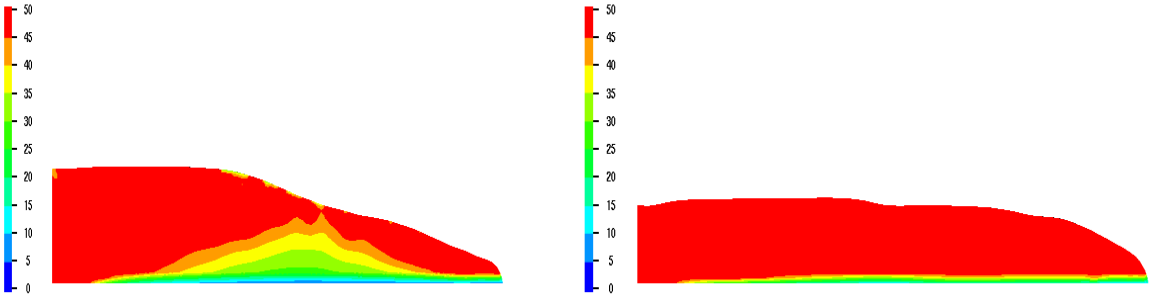

Figure 7: Effective viscosity μ_ε on midplane profile at times $t = 0.6s$ and $t = 1s$ for the same problem setup as in fig. 6.

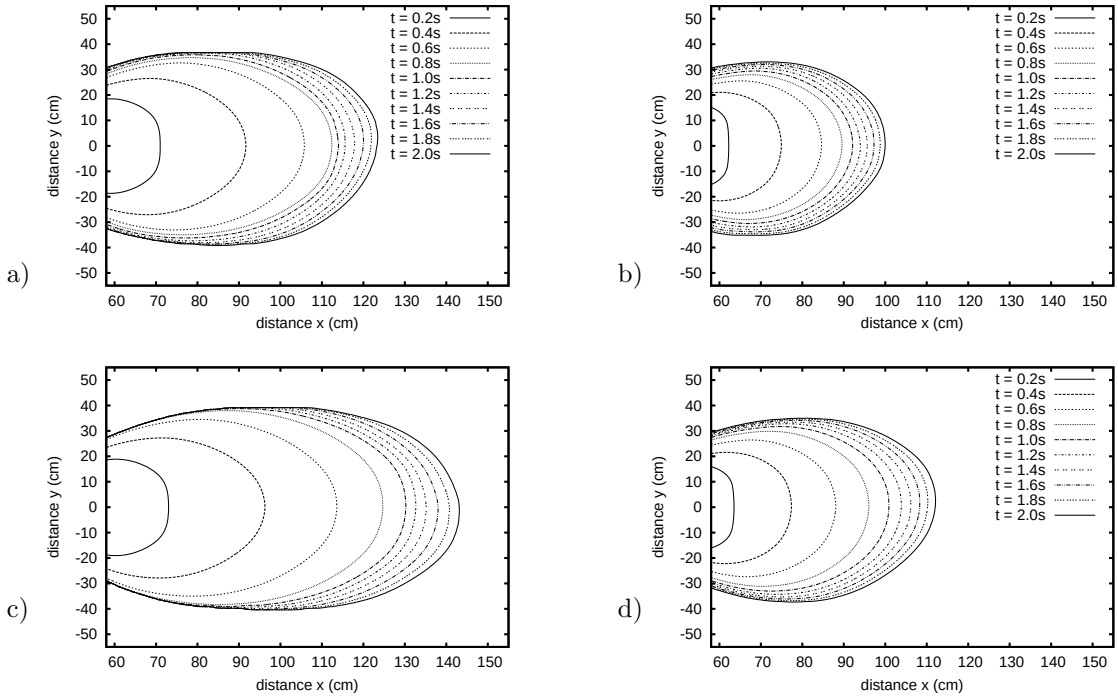

Figure 8: Contact line at times $t = 0.2\,k$ (s), $k = 1, \ldots, 10$ for a) $\alpha = 12^o$, $K = 47.68 Pas^{-n}$, $n = 0.415$, $\tau_s = 89Pa$, b) $\alpha = 12^o$, $K = 75.84 Pas^{-n}$, $n = 0.579$, $\tau_s = 109Pa$, c) $\alpha = 18^o$, $K = 47.68 Pas^{-n}$, $n = 0.415$, $\tau_s = 89Pa$, d) $\alpha = 18^o$, $K = 75.84 Pas^{-n}$, $n = 0.579$, $\tau_s = 109Pa$.

We note that in the previous numerical studies of the dam-break problem, the whole bulk of fluid was assumed to be released instantaneously (as in figure 6), i.e. the time needed for the gate to open was neglected. In the present approach we are able to model the gradual removal of the gate as well. In [13] the gate was rased within $t = 0.8s$, which is not negligibly small time. Numerical results shown below were computed for the gate opened within $0.8s$. We found this detail important for good comparison with experimental results.

Figures 8 and 9 show the evolution of the contact line of the free-surface over the inclined plane and of the flow-depth profile at the midplane. We note that the fluid attains fast initial motion and sharply decelerates around $t = 0.8$. Further the fluid front evolves gradually and slowly. We note that such two-fold behavior of numerical solution corresponds perfectly well to the experimental observations. In particular, describing the overall flow dynamics in experiments with Carbopol gel the authors of [13] stated "... we observed two regimes: at the very beginning ($t < 1s$), the flow was in an inertial regime; the front velocity was nearly constant. Then, quite abruptly, a pseudo-equilibrium regime occurred, for which the front velocity decayed as a power-law function of time." Since we stop our simulation at $t = 2s$, we are not able to recover the asymptotic decay of the front velocity (the time scale of the real-life experiment was about 8 hours). Nevertheless, the computed contact line plots and midplane profiles (shown in figures 8 and 9) compare well to the same statistics given in [13] for times $t \in \{0.2, 0.4, 0.6, 0.8, 1.0\}s$. In general, it should be noted that any viscoplastic model is an idealization of the possibly complex rheology of such fluid as Carbopol gel and certain deviation of numerical and experimental data is not unexpected.

4.3 Oscillating droplet problem

We consider a viscoplastic droplet for which evolution is driven only by surface tension forces. The fluid is assumed to be in rest at time $t = 0$ and $\mathbf{f} = \mathbf{0}$. The initial shape of the droplet is a perturbation of a sphere. In spherical coordinates (r, θ, φ) the initial shape is given by

$$r = r_0(1 + \widetilde{\varepsilon} S_2(\frac{\pi}{2} - \theta)),$$

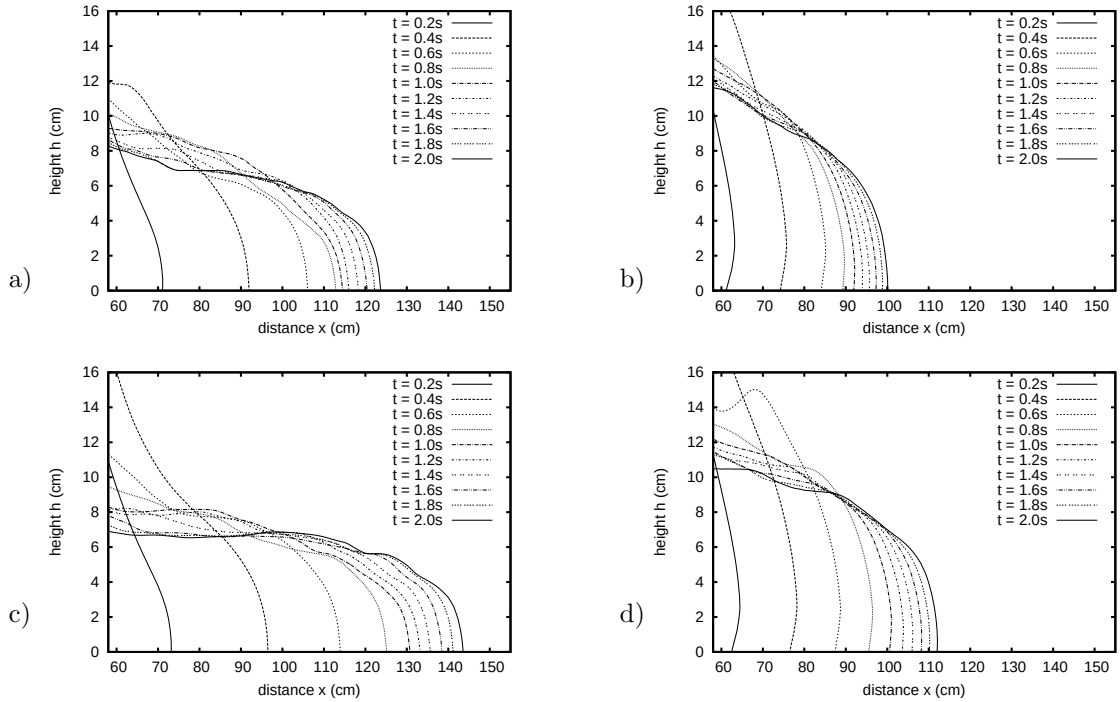

Figure 9: Midplane flow-depth profiles at times $t = 0.2\,k$ (s), $k = 1, \ldots, 10$ for a) $\alpha = 12^o$, $K = 47.68 Pas^{-n}$, $n = 0.415$, $\tau_s = 89Pa$, b) $\alpha = 12^o$, $K = 75.84 Pas^{-n}$, $n = 0.579$, $\tau_s = 109Pa$, c) $\alpha = 18^o$, $K = 47.68 Pas^{-n}$, $n = 0.415$, $\tau_s = 89Pa$, d) $\alpha = 18^o$, $K = 75.84 Pas^{-n}$, $n = 0.579$, $\tau_s = 109Pa$.

where S_2 is the second spherical harmonic. In all experiments we set $r_0 = 1$, $\varsigma = 1$ (surface tension), $\widetilde{\varepsilon} = 0.3$, and $K = 1/150$. At $t = 0$ the mean curvature of the surface is not constant, and an unbalanced surface tension force causes droplet oscillation. In this experiment the fluid motion is solely driven by the surface tension forces. Therefore, the quality of the numerical solution is sensitive to the accuracy of the level set function and surface curvature approximations. The oscillating droplet problem often serves as a benchmark test for free surface and two-phase flow solvers for the Newtonian fluids, see e.g. [8, 17, 23, 25, 45, 50]. However, we are not aware of any computational results for viscoplastic fluids. We present first results below. In the Newtonian regime, two statistics are of common interest: The droplet oscillation period T and the damping factor δ. In this case and for $\widetilde{\varepsilon} \ll 1$, a linear stability analysis from [34] predicts the period and the damping factor according to

$$T_{\text{ref}} = 2\pi\sqrt{\frac{\rho r_0^3}{8\varsigma}}, \qquad \delta_{\text{ref}} = \frac{2r_0^2}{5K}. \tag{18}$$

In general, this analysis is not necessarily valid for non-Newtonian fluids. For the viscoplastic case one may be interested in the cessation time T_f, e.g. the time when the system reaches the arrested state.

We solved the problem on a sequence of meshes with $h_{\min} \in \{\frac{1}{64}, \frac{1}{128}, \frac{1}{256}\}$ and the constant coarse mesh sizes $h_{\max} = \frac{1}{16}$ (the coarsest mesh size in the fluid domain interior) and $h_{\text{ext}} = \frac{1}{16}$ (the coarsest mesh size in the fluid domain exterior). The top left picture in figure 10 shows the the droplet top tip trajectories on the z axes computed for the sequence of meshes for the Newtonian case, $\tau_s = 0$. The curve $z = r_\infty + c\exp(-\frac{t}{\delta})$ is fitted to the computed maximum values of the droplet top tip, where r_∞ is the radius of a spherical droplet with the same volume as the initial droplet, $c = 0.1827$ and $\delta = 16.2$. Compared to the reference damping factor δ_{ref} the fitting shows that the scheme introduces a certain amount of numerical dissipation (see further discussion in [45]).

Next we compute the problem for the Herschel-Bulkley fluid with index $n = 1$ (Bingham fluid) and $\tau_s \in \{0.02, 0.03, 0.04\}$. The top right picture in figure 10 shows the droplet top tip trajectories for the different values of the stress yield parameter τ_s. The bottom picture compares the kinetic energy decay of the oscillating

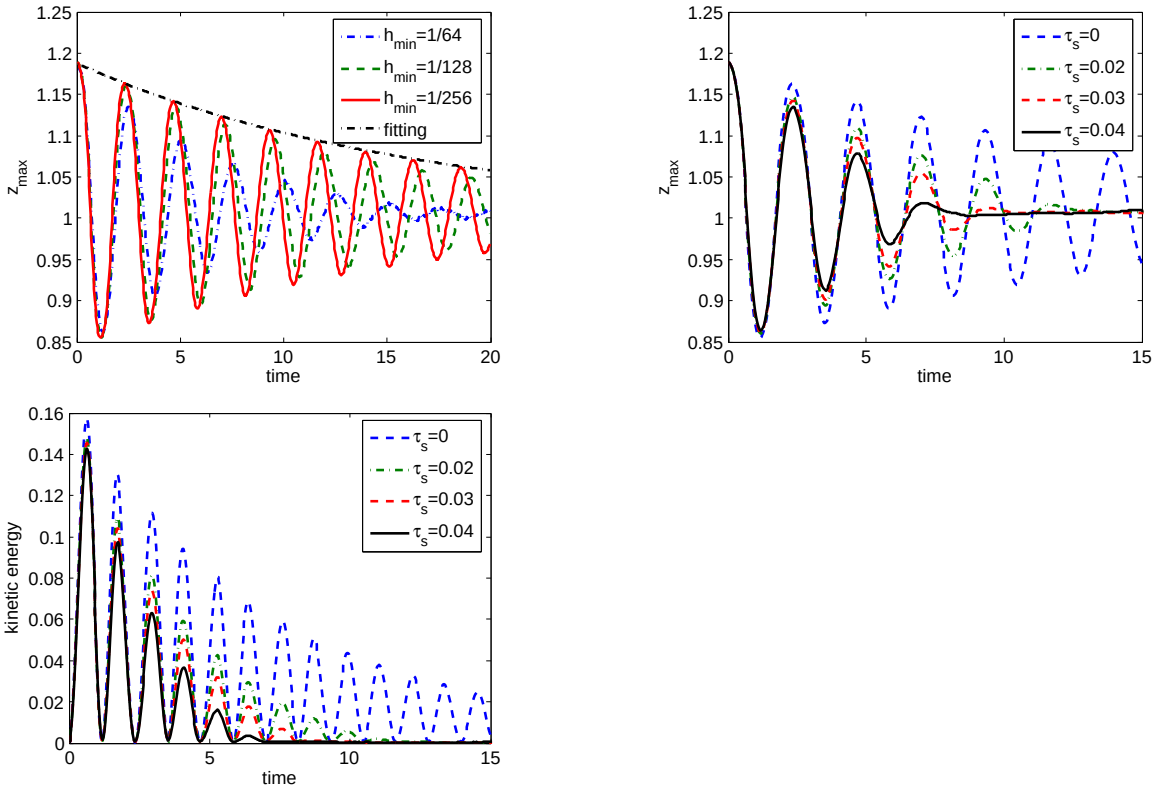

Figure 10: The top left picture shows the droplet top tip trajectories on the z axes for the sequence of meshes $h_{\min} \in \{1/64, 1/128, 1/256\}$ for the Newtonian case; The top right picture compares the droplet top tip trajectories for $\tau_s \in \{0, 0.02, 0.03, 0.04\}$ and $h_{\min} = 1/256$; The bottom picture compares the kinetic energy decay for different stress yield parameter values and $h_{\min} = 1/256$.

droplet for the different values τ_s. From the last two pictures it is well seen that for positive values of the stress yield parameter droplet oscillations prone to cease in a finite time. As well known from the theory of enclosed viscoplastic flows [28, 29] the cessation time T_f decreases for larger values of τ_s. The same tendency is observed for the oscillating droplet problem in figure 10. For regularized models, as one used in this paper, the fluid velocity, however, never decreases to zero in a finite time. If $\varepsilon > 0$, the cessation time T_f can be found approximately (of course, another level of uncertainty in the determination of T_f comes from the approximation error introduced by a numerical method, also for "ideal" viscoplastic models). We found approximate values of the cessation time $T_f = 12.8(\tau_s = 0.02)$, $T_f = 10.0(\tau_s = 0.03)$, and $T_f = 9.1(\tau_s = 0.04)$, using the following *ad hoc* criterium: T_f is a minimum time such that $E(t) < 5 \cdot 10^{-4}$ for all $t > T_f$, where $E(t)$ is the kinetic energy of the droplet. Another interesting observation from figure 10 is that the period is visually independent (or depends very weakly on) of the yield stress. Note that according to the linear analysis of the Newtonian case the period is independent of the viscosity, cf. (18). We are not aware if a similar property can be shown analytically in the non-Newtonian case.

5 Conclusions

We considered a numerical method for computing free surface flows of viscoplastic (Herschel-Bulkley) fluids. The method based on the level set function free surface capturing, on dynamically refined/coarsened octree cartesian grids, and semi-explicit splitting algorithm, has been shown to be an efficient approach to simulate such types of flows numerically. We tested the accuracy of the method in the Newtonian flow regime, when the

flow statistics can be compared with those available from experiment. Further we illustrate the performance of the method by computing several 3D viscoplastic fluid flows of interest: the flow over inclined planes for the dam-break problem and the freely oscillating droplet. The computed viscoplastic solutions demonstrate expected qualitative behavior and (for the dam-break problem) compare reasonably well with experimental data. We are not aware of other numerical simulations of fully 3D viscoplastic free surface flows with capillary forces. The reference [62] can be used to download the animated numerical solutions of the problems computed in the paper as well as few other animations of free surface (Newtonian and non-Newtonian) fluid flows, which illustrate the flexibility of the approach studied in the paper.

References

[1] D. Adalsteinsson, J.A. Sethian, The fast construction of extension velocities in level set methods, J. Comput. Phys. 148 (1999) 2–22.

[2] A.N. Alexandrou, E. Duc, V. Entov, Inertial, viscous and yield stress effects in Bingham fluid filling of a 2D cavity, J. Non-Newton. Fluid Mech. 96 (2001) 383–403.

[3] C. Ancey, Plasticity and geophysical flows: a review, J. Non-Newtonian Fluid Mech. 142 (2007) 4–35.

[4] Ch. Ancey, S. Cochard, The dam-break problem for Herschel-Bulkley viscoplastic fluids down steep flumes, J. Non-Newtonian Fluid Mech. 158 (2009) 18–35.

[5] N.J. Balmforth, R.V. Craster, A consistent thin–layer theory for Bingham plastics, J. Non-Newtonian Fluid Mech. 84 (1999) 65–81.

[6] N. J. Balmforth, R. V. Craster, A. C. Rust, R. Sassi, Viscoplastic flow over an inclined surface, J. Non-Newtonian Fluid Mech. 139 (2006) 103–127.

[7] N. Balmforth, S. Ghadgeb, T. Myers, Surface tension driven fingering of a viscoplastic film, J. Non-Newtonian Fluid Mech. 142 (2007) 143–149.

[8] E. Bänsch, Finite element discretization of the Navier-Stokes equations with a free capillary surface, Numer. Math. 88 (2001) 203–235.

[9] M. Behr, Stabilized space-time finite element formulations for free surface flows, Comm. Numer. Meth. Engrg. 11 (2001) 813–819.

[10] M. Bercovier and M. Engelman, A finite element method for incompressible non-Newtonian flows, J.Comp.Phys., 36 (1980), pp. 313–326.

[11] E. Bertakis, S. Gross, J. Grande, O. Fortmeier, A. Reusken, A. Pfennig, Validated simulation of droplet sedimentation with finite-element and level-set methods, Chem. Eng. Science 65 (2010) 2037–2051.

[12] A. Chorin, Numerical solution of the Navier-Stokes equations. Math. Comp., 22 (1968) 745–762.

[13] S. Cochard, C. Ancey, Experimental investigation of the spreading of viscoplastic fluids on inclined planes, J. Non-Newtonian Fluid Mech. 158 (2009) 73–84.

[14] P. Coussot, Mudflow Rheology and Dynamics, Balkema, Rotterdam, 1997.

[15] R. Croce, M. Griebel, M. A. Schweitzer, A parallel level-set approach for two-phase flow problems with surface tension in three space dimension, Preprint 157, Universitat Bonn, 2004.

[16] M. A. Cruchaga, D. J. Celentano, T. E. Tezduyar, Collapse of a liquid column: numerical simulation and experimental validation, Comput. Mech. 39 (2007) 453–476.

[17] M. Dai, H. Wang, J. B. Perot, D. P. Schmidt, Direct Interface Tracking of Droplet Deformation, Atomization and Sprays, 12 (2002) 721–735.

[18] E. J. Dean, R. Glowinski, G. Guidoboni, On the numerical simulation of Bingham visco-plastic flow: Old and new results, J. Non-Newtonian Fluid Mech., 142 (2007) 36–62.

[19] J. Dent, T. Lang, Experiments on the mechanics of flowing snow, Cold Regions Sci. Technol. 5 (1982) 243–248.

[20] G. Duvaut and J. L. Lions, Inequalities in Mechanics and Physics, Springer, 1976.

[21] P. Esser, J. Grande, A. Reusken, An extended finite element method applied to levitated droplet problems, Int. J. for Numer. Meth. in Engineering (2010). DOI: 10.1002/nme.2913

[22] I.A.Frigaard, C.Nouar, On the usage of viscosity regularization methods for viscoplastic fluid flow computation, J.Non-Newtonian Fluid Mech. 127 (2005) 1–26.

[23] M.M. Francois, S.J. Cummins, E.D. Dendy, D.B. Kothe, J.M. Sicilian, M.W. Williams, A balanced-force algorithm for continuous and sharp interfacial surface tension models within a volume tracking framework, J. Comput. Phys. 213 (2006) 141–173.

[24] T. P. Fries, The intrinsic XFEM for two-fluid flows, Int. J. Numer. Meth. Fluids 60 (2009) 437–471.

[25] S. Ganesan, L. Tobiska, An accurate finite element scheme with moving meshes for computing 3D-axisymmetric interface flows, Int. J. Numer. Meth. Fluids 57 (2008) 119–138.

[26] I. Ginzburg, K. Steiner, A free-surface lattice Boltzmann method for modelling the filling of expanding cavities by Bingham fluids, Phil. Trans. R. Soc. Lond. A 360 (2002) 453–466.

[27] I. Ginzburg, G. Wittum, Two-Phase Flows on Interface Refined Grids Modeled with VOF, Staggered Finite Volumes, and Spline Interpolants, J. Comput. Phys. 166 (2001) 302–335.

[28] R. Glowinski, Numerical Methods for Nonlinear Variational Problems, Springer-Verlag, New York, 1984.

[29] R.R. Huilgol, B. Mena, J.M. Piau, Finite stopping time problems and rheometry of Bingham fluids, J. Non-Newtonian Fluid Mech. 102 (2002) 97–107.

[30] R.W. Griffiths, The dynamics of lava flows, Annu. Rev. Fluid Mech. 32 (2000) 477–518.

[31] F. Harlow, J. Welch. Numerical calculation of time-dependent viscous incompressible flow of fluid with free surface. Phys. Fluids, 8 (1965) 2182-2189.

[32] A.J. Hogg, G.P. Matson, Slumps of viscoplastic fluids on slopes, J. Non-Newtonian Fluid Mech. 158 (2009) 101–112.

[33] G. Karapetsas, J. Tsamopoulos, Transient squeeze flow of viscoplastic materials, J. Non-Newtonian Fluid Mech. 133 (2006) 35–56.

[34] H. Lamb, Hydrodynamics, Cambridge University Press, 1932.

[35] J.-O. Lachaud, Topologically defined iso-surfaces. DGCI (1996) 245–256.

[36] V. Lebedev, Difference analogues of orthogonal decompositions, basic differential operators and some boundary problems of mathematical physics, I,II. U.S.S.R. Comput. Math. Math. Phys., 4(3) (1964) 69–92, 4(4) (1964) 36–50.

[37] W. Lorensen, H. Cline, Marching Cubes: A High Resolution 3D Surface Construction Algorithm, Computer Graphics, 21 (1987) 163–169.

[38] F. Losasso, F. Gibou, R. Fedkiw, Simulating water and smoke with an octree data structure, ACM Transactions on Graphics (TOG), 23 n.3, August 2004.

[39] J. Martin, W. Moyce, An experimental study of the collapse of liquid columns on a rigid horizontal plane, Philos.Trans.R.Soc.Lond.Ser.A 244 (1952) 312–324.

[40] D. Meagher, Geometric modeling using octree encoding, Computer Graphics and Image Processing, 19 (1982) 129–147.

[41] C. Min, F. Gibou, A second order accurate level set method on non-graded adaptive cartesian grids, J. Comput. Phys. 225 (2007) 300–321.

[42] F. Mut, G.C. Buscaglia, E.A. Dari, A new mass-conserving algorithm for level set redistancing on unstructured meshes, Mecanica Computacional 23 (2004) 1659–1678.

[43] Q.D. Nguyen, D.V. Boger, Measuring the flow properties of yield stress fluids, Annu. Rev. Fluid Mech. 24 (1992) 47–88.

[44] K.D. Nikitin, Y. V. Vassilevski, Free surface flow modelling on dynamically refined hexahedral meshes, Rus. J. Numer. Anal. Math. Model., 23 (2008) 469–485.

[45] K.D. Nikitin, M.A. Olshanskii , K.M. Terekhov, Y. V. Vassilevski, Numerical simulations of free surface flows on adaptive cartesian grids with level set function method, Preprint is available online, 2010.

[46] S. Osher, R. Fedkiw, Level Set Methods and Dynamic Implicit Surfaces. Springer-Verlag, 2002.

[47] E. Oñate, S. Idelsohn, O.C. Zienkiewicz and R.L. Taylor - A Finite Point Method in Computational Mechanics. Applications to Convective Transport and Fluid Flow, Int. J. Num. Meth. Eng. 39 (1996) 3839–3866

[48] T. C. Papanastasiou, Flows of materials with yield, J.Rheol., 31 (1987) 385–404.

[49] S. Popinet, An accurate adaptive solver for surface-tension-driven interfacial flows, J. Comput. Phys. 228 (2009) 5838–5866.

[50] S. Quan, D. Schmidt, A moving mesh interface tracking method for 3D incompressible two-phase flows, J J. Comput. Phys. 221 (2007) 761–780.

[51] H. Samet, The Design and Analysis of Spatial Data Structures, Addison-Wesley, New York, 1989.

[52] H. Samet, Applications of Spatial Data Structures: Computer Graphics, Image Processing and GIS, Addison-Wesley, New York, 1990.

[53] R. Scardovelli, S. Zaleski, Direct numerical simulation of free-surface and interfacial flow, Annual Review of Fluid Mechanics 31 (1999) 567–603.

[54] W.R. Schowalter, G. Christensen, Toward a rationalization of the slump test for fresh concrete: comparisons of calculations and experiments, J. Rheol. 42 (1998) 865–870.

[55] J.A. Sethian, Level Set Methods and Fast Marching Methods: Evolving Interfaces in Computational Geometry, Fluid Mechanics, Computer Vision, and Materials Science, Cambridge University Press, Cambridge, 1999.

[56] J. Strain, Tree Methods for Moving Interfaces, J. Comput. Phys. 151 (1999) 616–648.

[57] M. Sussman, P. Smereka, S. Osher, A level set approach for computing solutions to incompressible two-phase flow, J. Comput. Phys. 114 (1994) 146–159.

[58] J.Strain, Semi-Lagrangian methods for level set equations. J. Comput. Phys., 151 (1999) 498–533.

[59] R. Szeliski, Rapid octree construction from image sequences, CVGIP: Image Understanding, 58 (1993) 23–32.

[60] G. Tryggvason, B. Bunner, A. Esmaeeli, D. Juric, N. Al-Rawahi, W. Tauber, J. Han, S. Nas, and Y.-J. Jan. A front-tracking method for the computations of multiphase flow. J. Comput. Phys., 169 (2001) 708–759.

[61] Yue W., Lin C.L., Patel V.C., Numerical simulation of unsteady multidimensional free surface motions by level set method. Int J Numer Methods Fluids 42 (2003) 853–884.

[62] http://www.inm.ras.ru/research/freesurface